Available online at www.sciencedirect.com
ScienceDirect
Solid State Communications 144 (2007) 124–127
solid state communications
www.elsevier.com/locate/ssc

Temperature-modulated scanning tunneling spectroscopy of gold nanoparticle dropcast films

Shaowei Chen*, Li-Ping Xu, Sulolit Pradhan, Wei Chen

Department of Chemistry and Biochemistry, University of California, 1156 High Street, Santa Cruz, CA 95064, USA

Received 28 July 2007; accepted 8 August 2007 by A.H. MacDonald
Available online 15 August 2007

Abstract

The electronic conductivity of a gold nanoparticle dropcast film was examined by temperature-modulated scanning tunneling spectroscopy (STS). The low-conductance Coulomb blockade was found to shrink with increasing temperature, which at ambient temperature (ca. 290 K) diminished completely. Concomitantly, the potential spacing between adjacent peaks observed in the Coulomb staircase features exhibited a marked increase at approximately the same temperature. Both observations suggest an enhancement of the particle film electronic conductivity with increasing temperature. Such a transition was ascribed to the combined consequence of thermal activation of interparticle charge transfer and particle coherent thermal motions.

PACS: 73.63.-b

Keywords: A. Thin films; A. Nanostructures; C. Scanning tunneling microscopy; D. Electronic transport

1. Introduction

The extensive research interest in nanosized particles has been primarily motivated by their potential applications as the new building blocks for the fabrication of next-generation electronic devices and circuitries. In these efforts, an understanding of the particle-charge-transfer properties represents a critical first step. So far a majority of research activities have been focused on a unique class of nanoparticle materials, the monolayer-protected nanoclusters (MPCs) [1–3], that exhibit room-temperature Coulomb staircase in scanning tunneling spectroscopic (STS) measurements [4] and quantized charging characters in solution electrochemistry [5]. More recently, with deliberate control of the nanoparticle structure and assemblies, lateral single electron transfer (SET) was also observed in electrochemical studies of nanoparticle Langmuir–Blodgett (LB) thin films [6]. Interestingly, the solid-state SET only occurred when the temperature was above a certain threshold. While thermal activation has been proposed as the predominant charge-transfer mechanism in the interpretation of the electronic conductivity properties of nanoparticle solids [7–9], recent studies suggest that thermally induced physical motions of the particles may also play an important role [10]. This is ascribed to the temperature-modulated interparticle separation as a consequence of the coherent physical displacements of the cores. In fact, low-frequency Raman scattering studies have shown that nanoparticle solids may exhibit vibrational collective coherence, with the frequency inversely proportional to the particle core diameter [11]. Yet, the mechanistic details remain to be explored.

In this article, we report the temperature-modulated STS measurements of nanoparticle solid films prepared by the dropcast method, which serve as a nanoscale structural analogue to the particle LB monolayers in that the ensemble conductance is measured both in the two-electrode mode involving interparticle electron hopping (see Fig. 2, panels B and C). A clear transition from low to high conductance can be seen in the particle thin films with increasing temperature; and the transition temperature appears to be consistent with that observed previously [6] with nanoparticle LB monolayers deposited onto an interdigitated array (IDA) electrode.

* Corresponding author.
E-mail address: schen@chemistry.ucsc.edu (S. Chen).

0038-1098/$ - see front matter © 2007 Elsevier Ltd. All rights reserved.
doi:10.1016/j.ssc.2007.08.008

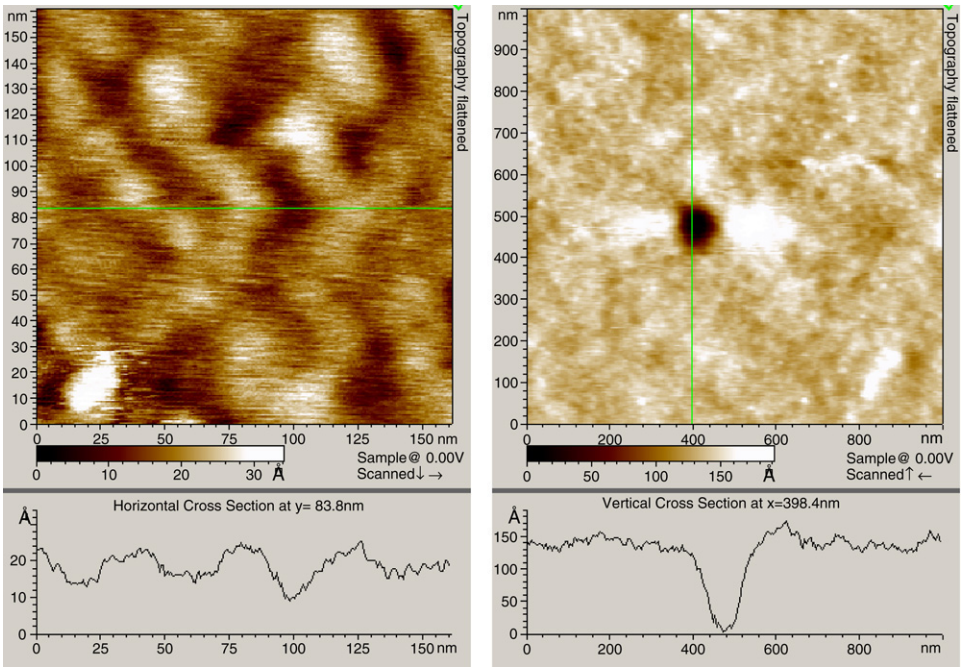

Fig. 1. AFM topographic images and line scans of C10Au nanoparticle thin films on C10S SAM/Au(111). Note that the scales are different in these two images.

2. Experimental section

Chemicals. Tetra-n-octylammonium bromide (98%, Aldrich), 1-decanethiol (C10SH, 96%, ACROS), and sodium borohydride ($NaBH_4$, 98%, ACROS) were all used as received. Hydrogen tetrachloroauric acid ($HAuCl_4$) was synthesized by dissolving ultra-high purity gold (99.999%, Johnson Matthey) in freshly prepared aqua regia. Water was supplied by a Barnstead Nanopure water system (18.3 MΩ). All solvents were purchased from typical commercial sources and used as received.

Nanoparticle synthesis. 1-Decanethiolate-protected gold nanoparticles (C10Au) were synthesized by using the modified Brust reaction [1] followed by fractionation and thermal annealing to reduce the core size dispersity [2,3]. The fraction with core diameter of ca. 2.0 nm (as determined by transmission electron microscopic measurements) was used in the subsequent measurements.

Nanoparticle assemblies. Prior to the deposition of the particles, a Au(111) thin film on mica (from Molecular Imaging) was first cleaned in UV-ozone (Model 42, Jelight Co) for 10 min, and then coated with a decanethiol self-assembled monolayer (C10S SAM) by immersion into a 1 mM C10SH solution in ethanol for 24 h. A particle solid film was then formed on the substrate surface by dropcasting a concentrated solution of the C10Au nanoparticles in toluene onto the C10S SAM/Au(111) surface.

AFM measurements. AFM topographic images were acquired under ambient conditions with a PicoLE SPM instrument (Molecular Imaging) in the tapping mode. The uncoated silicon cantilevers exhibit resonant frequencies between 120 and 190 kHz (typically 165 kHz), force constants of 2.5–8.5 N/m, and tip apex radii of ∼10 nm. The resulting images were flattened and plane-fitted using software from Molecular Imaging.

STM/STS measurements. A mechanically cut Pt/Ir tip was used in the STM/STS measurements. A high impedance of 75 MΩ was used to prevent tip damage and capture of the particles (at bias 1.5 V, and set point 0.02 nA). STM topographic images were recorded in constant current mode. STS I–V data were collected in the spectroscopy mode with the feedback loop turned off. 200 data points were collected in a typical voltage sweep of ±2.5 V. Each I–V curve was averaged five times, from which the conductance (dI/dV) profiles were obtained. The particle thin film temperature was controlled by a Lakeshore Temperature Controller (Model 311).

3. Results and discussion

Fig. 1 shows a representative AFM topographic image of the particle assembly. From the line scans, the film was found to be rather smooth with an average thickness of ca. 15 nm (right panel). When zoomed in, the AFM image (left panel) clearly depicts arrays of nanoparticles. Assuming that the particle physical diameter is approximately 4.5 nm (core plus two fully extended C10S chains), this corresponds to about four layers of nanoparticles considering that ligand intercalation occurs between adjacent layers of particles [12].

STM and STS studies were then carried out. A representative STM topographic image acquired at room temperature in constant current mode was depicted in Fig. 2(A). It can be seen that the particle layer was quite dense with modest roughness, in agreement with the AFM measurements (Fig. 1). It should be noted that stable and reproducible images were obtained in repeated scans, indicating good immobilization of the particles by the C10S SAM and minimal perturbation of the particle layers by the STM tip [13]. I–V data were then collected in the spectroscopy mode.

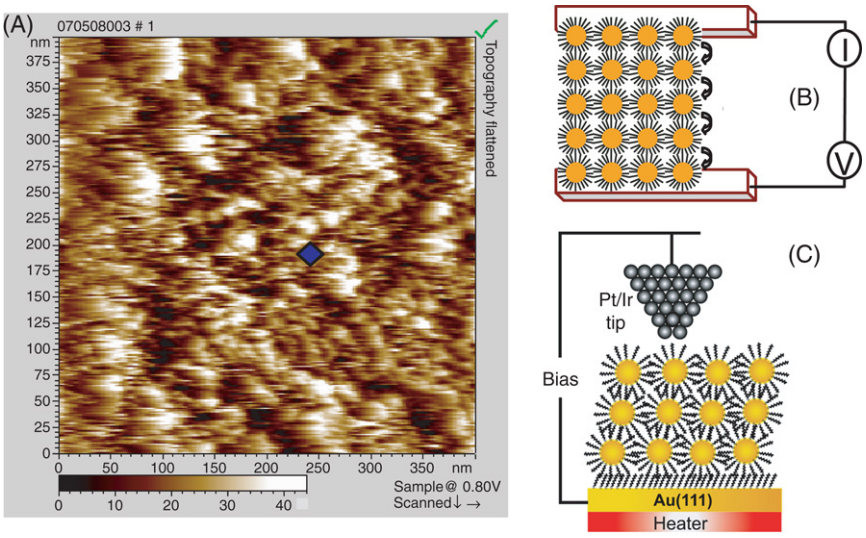

Fig. 2. (A) STM topographic image of a C10Au nanoparticle thin film deposited onto C10S SAM/Au(111). Blue diamond marks the tip position for STS measurements. (B) Schematic of conductivity measurements of a nanoparticle LB monolayer by voltammetric techniques; and (C) STS study of a nanoparticle dropcast film. (For interpretation of the references to colour in this figure legend, the reader is referred to the web version of this article.)

Fig. 3 shows some representative conductance (dI/dV) profiles at varied temperatures by parking the tip on a randomly selected position of the particle film surface (marked by a diamond in Fig. 2(A)). Two aspects warrant attention here. First, at low temperatures (<20 °C, bottom panel), the conductance profiles exhibit a flat central region beyond which well-defined Coulomb staircase features start to emerge; whereas at higher temperatures (≥20 °C, top panel), only the Coulomb staircase features can be seen. The appearance of the low-conductance Coulomb blockade is consistent with the semiconductor characters that arise from the organic/inorganic composite nature of the particles. It should be cautioned that the particles under study are too big in size to exhibit a meaningful bandgap [5]. Interestingly, with increasing temperature, this gap shrinks, and at higher temperatures (≥20 °C, top panel), it disappears altogether. The details are depicted in Fig. 4 (□), where the error bars reflect the statistical average of more than 20 I–V curves at each temperature. It can be seen that the gap is ~0.6 V at $T < 20$ °C but diminishes rapidly at $T \geq 20$ °C. This suggests enhanced conductance of the nanoparticle films with increasing temperature. Qualitatively, this observation is in agreement with previous solid-state electrochemical measurements of the conductivity properties of nanoparticle dropcast thick films [7–9]. It was accounted for by the increasing number of electronic states that contributed to interparticle charge transfer, as a consequence of the thermal activation mechanism.

The above observation is also consistent with the Coulomb staircase measurements. Fig. 4 shows the variation of the average peak spacing (ΔV, Fig. 3) with temperature (●). Again, the error bars reflect the statistical average of peak spacing of more than 20 I–V curves at each temperature. A transition at 20–25 °C can be clearly seen, which coincides with that in the gap measurements. At low temperatures (<20 °C), ΔV is about 0.6 V; whereas at higher temperatures (≥25 °C), it increases to about 1.1 V. The increase in ΔV suggests a decrease in the effective capacitance of the junction between the STM tip and the Au(111) substrate (Fig. 2(C)), which is presumably dominated by the capacitance of the particle

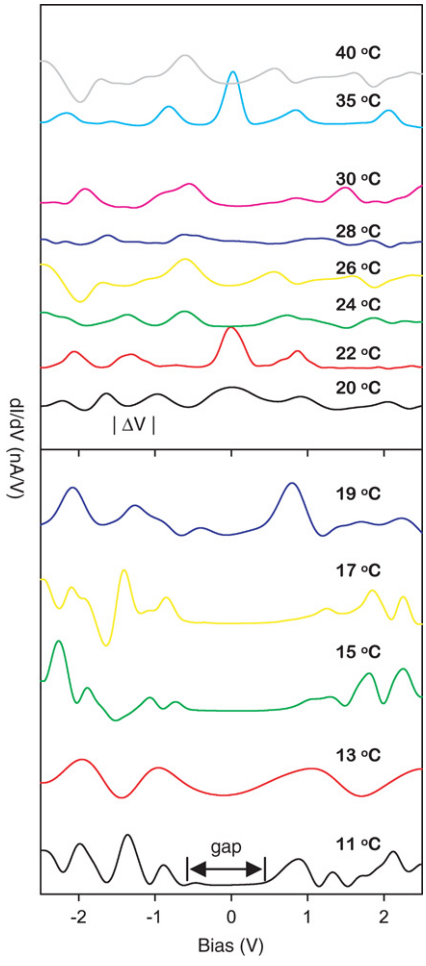

Fig. 3. STS dI/dV profiles of C10Au nanoparticles on C10S SAM/Au(111) within the temperature range of 11–40 °C.

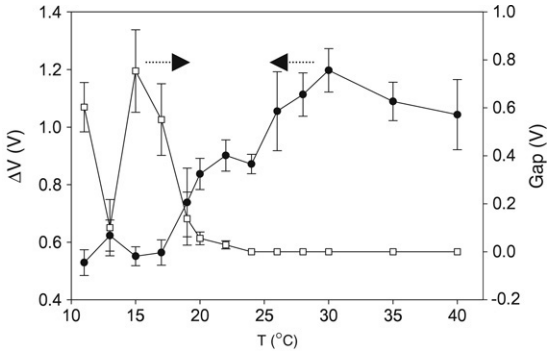

Fig. 4. Averaged potential spacing (ΔV, •) between adjacent peaks and Coulomb blockade gap (□) at different temperatures. Data are acquired from the dI/dV curves as exemplified in Fig. 3. Each data point is the statistic average of more than 20 measurements.

layers. This can be, at least in part, attributed to the decrease in permittivity of the particle ensembles with increasing temperature, rendering the resistive components more dominant in the double junctions, again, in accordance with the enhanced conductance as reflected in the gap measurements.

Yet, it should be emphasized that the transition temperature observed above (20–25 °C) is substantially higher than that estimated in differential scanning calorimetry (DSC) measurements of the C10Au nanoparticles (∼ −8 °C) [12]. Additionally, in our earlier studies [6] with LB monolayers of hexanethiolate-passivated gold (C6Au) nanoparticles (Fig. 2(B)), the solid-state SET was observed only at T = 20–25 °C, with a sudden increase in the ensemble conductance (by several orders of magnitude) as compared to that at lower temperatures. The similarity of the transition temperature between these two vastly different particle systems and experimental setups strongly suggests that the abrupt change of the ensemble conductivity cannot be accounted for by the melting of the alkyl ligands alone, and additional contributions most probably arise from thermal motions of the particle cores [10].

As a first-order approximation, the interparticle-charge-transfer rate constant increases exponentially with temperature (Arrhenius law), whereas the particle thermal vibrational frequency is anticipated to decrease with temperature (as a consequence of weakened interparticle interactions with increasing temperature). Thus, at low temperature, contribution of the latter to the particle ensemble conductance is minimal as the interparticle charge transfer is mainly limited by thermal activation. With the increase in temperature, the frequency of the particle thermal motions becomes comparable to the interparticle-charge-transfer rate, and thus both make a meaningful contribution to the ensemble conductance. For instance, in low-frequency Raman scattering measurements, at room temperature the particle coherent vibrational motions typically exhibit a frequency of a few tens of wavenumber, or 10^{10}–10^{11} s^{-1} [11]. And in previous studies of solid-state SET of nanoparticle monolayers [6], the electron-transfer rate constant is found to be of the order of 10^{10}–10^{11} s^{-1} at ambient temperature; whereas at lower temperatures, the rate constant drops by several orders of magnitude. Therefore, the transition from low to high conductance occurs around this temperature. This hypothesis is currently being further examined by computational and spectroscopic measurements.

4. Conclusion

Temperature-modulated scanning tunneling spectroscopy was carried out to examine the conductivity properties of gold nanoparticle solid films. A clear transition from low to high conductance was observed at around ambient temperature, as manifested in Coulomb blockade and staircase measurements. The enhanced conductivity may be accounted for by the combined consequence of thermally activated interparticle charge transfer and particle vibrational collective coherence.

Acknowledgment

This work was supported in part by the National Science Foundation (CHE-0456130 and CHE-0718170).

References

[1] M. Brust, M. Walker, D. Bethell, D.J. Schiffrin, R. Whyman, Journal of the Chemical Society - Series Chemical Communications (1994) 801–802.
[2] R.L. Whetten, M.N. Shafigullin, J.T. Khoury, T.G. Schaaff, I. Vezmar, M.M. Alvarez, A. Wilkinson, Accounts of Chemical Research 32 (1999) 397–406.
[3] A.C. Templeton, M.P. Wuelfing, R.W. Murray, Accounts of Chemical Research 33 (2000) 27–36.
[4] R.P. Andres, T. Bein, M. Dorogi, S. Feng, J.I. Henderson, C.P. Kubiak, W. Mahoney, R.G. Osifchin, R. Reifenberger, Science 272 (1996) 1323–1325.
[5] S.W. Chen, R.S. Ingram, M.J. Hostetler, J.J. Pietron, R.W. Murray, T.G. Schaaff, J.T. Khoury, M.M. Alvarez, R.L. Whetten, Science 280 (1998) 2098–2101.
[6] S. Pradhan, J. Sun, F.J. Deng, S.W. Chen, Advanced Materials 18 (2006) 3279–3283.
[7] W.P. Wuelfing, R.W. Murray, Journal of Physical Chemistry B 106 (2002) 3139–3145.
[8] F.J. Ibanez, F.P. Zamborini, Langmuir 22 (2006) 9789–9796.
[9] R.C. Doty, H.B. Yu, C.K. Shih, B.A. Korgel, Journal of Physical Chemistry B 105 (2001) 8291–8296.
[10] J.P. Choi, M.M. Coble, M.R. Branham, J.M. DeSimone, R.W. Murray, Journal of Physical Chemistry C 111 (2007) 3778–3785.
[11] M.P. Pileni, Accounts of Chemical Research 40 (2007) 685–693.
[12] M.J. Hostetler, R.W. Murray, Current Opinion in Colloid & Interface Science 2 (1997) 42–50.
[13] G.H. Yang, L. Tan, Y.Y. Yang, S.W. Chen, G.Y. Liu, Surface Science 589 (2005) 129–138.